PAPER • OPEN ACCESS

Optimizing detachment control using the magnetic configuration of divertors

To cite this article: C. Cowley *et al* 2022 *Nucl. Fusion* **62** 086046

OPEN ACCESS
IOP Publishing | International Atomic Energy Agency Nuclear Fusion
Nucl. Fusion **62** (2022) 086046 (19pp) https://doi.org/10.1088/1741-4326/ac7a4c

Optimizing detachment control using the magnetic configuration of divertors

C. Cowley[1,*], B. Lipschultz[1], D. Moulton[2] and B. Dudson[1,3]

[1] York Plasma Institute, University of York, Heslington, York YO10 5DQ, United Kingdom
[2] UKAEA-CCFE, Culham Science Centre, Abingdon OX14 3DB, United Kingdom
[3] Lawrence Livermore National Laboratory, 7000 East Ave., Livermore, CA 94550, United States of America

E-mail: czlc500@york.ac.uk

Received 21 February 2022, revised 24 May 2022
Accepted for publication 20 June 2022
Published 6 July 2022

Abstract

As tokamak research moves to reactor conditions, the control of a stable, optimally-detached divertor plasma has become increasingly relevant. Simple predictions of such detachment control have been performed previously using the detachment location sensitivity (DLS) model (Lipschultz *et al* 2016 *Nucl. Fusion* **56** 056007). In this study the DLS model is extended and combined with SOLPS-ITER simulations of isolated divertor grids to study the effects of alternate divertor magnetic field properties on detachment control. The DLS model predicts that divertors can achieve easier access to detachment through a long connection length, a high total flux expansion, and a high average magnetic field in the divertor compared with that at the *x*-point. SOLPS-ITER simulations suggest an even stronger impact of total flux expansion and connection length on detachment access than the DLS model predicts. In terms of detachment evolution, both simulation and modelling show a high gradient in the total magnetic field and low $\frac{B_{\mathrm{pol}}}{B}$ are able to more easily keep a detachment front at a desired poloidal location. Regions with no stable detachment front locations can arise for high magnetic field gradients directed towards the target. Significant differences have been found between impurity scan simulations and the DLS model. These differences may be attributed to sources and sinks of power and electron pressure, and should be explored further in future work.

Keywords: detachment, divertors, edge physics, advanced divertors, SOL, SOLPS, detachment control

(Some figures may appear in colour only in the online journal)

1. Introduction

In the field of magnetic confinement fusion research, tokamaks are currently transitioning from smaller scale experiments to large reactor-like machines. These machines include tokamaks such as ITER, DEMO, and the Spherical Tokamak for Energy Production (STEP) [2–4], and are all expected to pose significant challenges for the plasma facing components. In fact, un-mitigated heat fluxes on the ITER and DEMO divertor surfaces are expected to exceed the engineering limits of divertor tiles without control over the plasma exhaust [5, 6].

In an attempt to reduce the power and particle loads of tokamaks, many physicists have proposed operating with 'advanced' or 'alternative' divertors. These are divertor configurations that have been suggested as having characteristics that aid control of plasma exhaust in some way. Such characteristics include: (a) higher order *x*-points, which can be seen in 'snowflake' configurations [7]; longer connection lengths, which are the defining features of 'X-divertors' [8]; and (c) and high total flux expansions resulting from low total magnetic fields at the target, which can be seen in Super-X divertors [9]. Each of these features have unique proposed benefits for

* Author to whom any correspondence should be addressed.

plasma exhaust, including increased spreading of heat loads, or lower target temperatures. One of the most crucial proposed effects of advanced divertors is how they are able to influence the mode of divertor operation known as detachment.

There exist many regimes for divertor plasmas, and of these the regime of detachment is ideal for mitigating damage caused by plasma exhaust. Fundamentally, a detached divertor is one where a high power, high temperature plasma terminates at some point before reaching the divertor targets, leaving a relatively cold low pressure region of partially ionised gas towards the target. Because the high temperature plasma is not in direct contact with the targets, the plasma is said to have 'detached' from the target [10].

More specifically, detachment is typically characterised by a sharp drop in heat flux and temperature over a region upstream of the divertor target, referred to as the thermal front [10]. Upstream of this position is a high temperature, high pressure, heat conduction-dominated plasma. Downstream lies the detached region, which consists of a cold ($T_e < 5$ eV), low pressure, heat convection-dominated partially ionised gas. This regime is in stark contrast to attached divertors, in which significant drops in heat flux and pressure are only seen very near to the divertor target, if at all.

In experiment, detachment is typically achieved through changes in some 'control' parameter(s) affecting power balance in the divertor; including upstream plasma density, power entering the scrape off layer (SOL), or the concentration of impurities in the divertor plasma [11, 12]. In addition to initiating detachment at the target, these parameter can also force a movement in the thermal front away from or towards the target, making more or less of the divertor region detached. Having the thermal front at the target is not necessarily advantageous, since it may not sufficiently spread power loads and can easily reattach. On the other hand, a thermal front near the x-point may lead to a reduction in performance of the core plasma. Because of this, an important aspect of the design of next-generation tokamaks is to find and hold the thermal front at a point that both optimizes target power reduction and minimizes core performance degradation.

To assess the full potential of advanced divertor configurations, it is of paramount importance to understand how the magnetic configuration of a divertor influences access to and control over detachment. Much of the current work in this area consists of 1D models that predict what divertor features may be important in detachment [1], and full-geometry simulations of detachment in advanced divertors [13]. These full-geometry simulations can predict whether detachment control is better or worse in some configurations. However, in these simulations it is often difficult to discern which physical effects or geometric features lead to the differences in detachment control, and whether these agree with 1D modelling. As such, this study aims to extend the detachment location sensitivity (DLS) model, and compare its predictions to simple SOLPS-ITER simulations of isolated divertors. The combination of this fundamental physics model and idealised 2D simulations should enhance our understanding of how we can optimise detachment characteristics using the magnetic configuration of divertors. This study also reveals disagreements between 1D models and SOLPS-ITER simulations. However, these are not investigated in detail here; instead we emphasise the simulated results and their applications to control over plasma exhaust. In the future, we hope to explore the model disagreements through extensions to the DLS model [14], or more in-depth SOLPS analysis.

2. Theoretical formulation of the DLS model

In this section we summarise the results of [1] relevant to the extensions in this paper. In particular, we cover a similar derivation of the DLS model introduced in [1], but refrain from specifying the exact form of the divertor magnetic field, and apply the derivation to an isolated divertor with no concern for physics upstream of the x-point.

Fundamentally, the DLS model is a one-dimensional model for heat balance upstream from the detached region in a divertor [15]. Using the Lengyel model for impurity radiation [16], parallel power balance between the upstream entrance of the divertor and the cold end of this thermal front (the forward end of the detached region) can be written [16]:

$$\frac{q_{\parallel,u}^2}{B_u^2} - \frac{q_{\parallel,c}^2}{B_c^2} = -f_\alpha \int_{s_{\parallel,c}}^{L_\parallel} \frac{2q_\parallel (n^2 L_\alpha(T) + S_0)}{B^2} \mathrm{d}s_\parallel, \qquad (1)$$

where $q_\parallel$ is the parallel electron heat flux density, B is the total magnetic field strength, n is the electron density, $L_\alpha(T)$ is the electron cooling function of impurity α, T is the electron temperature, S_0 contains non-impurity power sources or sinks, $s_\parallel$ is the parallel distance from the target, and $L_\parallel$ is the parallel connection length between the target and upstream divertor entrance. f_α is the fixed (over the thermal front region) fraction of impurity species α, defined by the ratio of the impurity density to that of the local electron density, $f_\alpha = \frac{n_\alpha}{n}$. Subscripts u and c denote the upstream entrance of the divertor, and the cold end of the thermal front respectively. Applying equation (1) to a detached divertor plasma, the heat flux leaving the cold end of the front should be negligible compared to that entering the upstream end of the flux tube at $L_\parallel$. Moreover, if it is assumed that all heat flux in the thermal front is electron conducted, and that impurities are the dominant sink of heat, then we can write $q_\parallel = -\kappa_1 T^{5/2} \frac{\mathrm{d}T}{\mathrm{d}s_\parallel}$ in the right-hand side integral and set $S_0 = 0$. Here, κ_1 is the Spitzer conductivity divided by $T^{5/2}$, which is typically taken approximated as a constant for a constant ion charge state Z [10]. Under these assumptions, equation (1) becomes

$$\frac{q_{\parallel,u}^2}{B_u^2} = 2\kappa_1 f_\alpha \int_{T_c}^{T_u} \frac{T^{5/2} n^2 L_\alpha(T)}{B^2} \mathrm{d}T. \qquad (2)$$

This expression can be simplified further by assuming that the thermal front is very thin, such that the hot and cold ends of the front are roughly in the same location. Under this approximation, we can use subscript f to denote the average position of the thermal front. Thus, B can be taken out of the integral in equation (2) as its value at f. Because this model centres around the thermal front, we also use the front location $s_{\parallel,f}$ to generally indicate the position of detachment. As a result, *we*

will henceforth refer to the thermal front and detachment front interchangeably. An additional assumption we can make is to assume constant electron pressure from the upstream to the front location[4], such that at any point in the detachment front the electron density can be written $n = \frac{n_u T_u}{T}$ [1]. The result is

$$q_{\parallel,u} = \frac{B_u}{B_f} n_u T_u f_\alpha^{1/2} \sqrt{2\kappa_1 \int_{T_c}^{T_u} T^{1/2} L_\alpha(T) \mathrm{d}T}. \tag{3}$$

Finally, T_u can be expressed as an explicit function of parallel distance $s_\parallel$ using the conduction equation, by assuming the temperature at the cold end of the front is sufficiently low:

$$T_u \approx \left[\frac{7}{2\kappa_1} \int_{s_{\parallel,f}}^{L_\parallel} q_\parallel(s_\parallel) \mathrm{d}s_\parallel \right]^{2/7}. \tag{4}$$

Here, because we have assumed power loss only over the detachment front, the conducted heat flux $q_\parallel$ in the divertor above the detachment front has a functional form $q_\parallel(s) = q_{\parallel,u} \frac{B}{B_u}$. Combining equations (4) and (3) with this form of $q_\parallel$ gives:

$$q_{\parallel,u} = n_u f_\alpha^{1/2} q_{\parallel,u}^{2/7} \frac{B_u}{B_f} \left[\frac{7}{2\kappa_1} \int_{s_f}^{L} \frac{B}{B_X} \mathrm{d}s_\parallel \right]^{2/7} \times \sqrt{2\kappa_1 f_\alpha \int_{T_{e,c}}^{T_u} T^{1/2} L_\alpha(T) \mathrm{d}T}. \tag{5}$$

It may be important to note that in equation (4) we are unable to take B outside of the integral, since the region where $q_\parallel(s)$ is finite spans a wide area from the divertor entrance to the front, across which B may vary significantly. Now given that the temperature range of the detachment front spans the effective limits of the cooling curve, then the right-most integral in equation (5) should be a constant regardless of the front location. Thus, the above expression is a relationship between detachment front location and control parameters such as f_α. This relationship is modulated only by constants, and on the divertor configuration (through B, $s_\parallel$, and $L_\parallel$). To show this explicitly, we can rearrange equation (5) to give:

$$C(s_{\parallel,f}) = \frac{n_u \sqrt{f_\alpha}}{q_{\parallel,u}^{5/7}} = C_0 \frac{B_f}{B_u} \left[\int_{s_{\parallel,f}}^{L_\parallel} \frac{B}{B_u} \mathrm{d}s_\parallel \right]^{-2/7}. \tag{6}$$

Here C is a lumped detachment control parameter required for a detachment front to be located at $s_{\parallel,f}$, and takes into account the effects of upstream electron density n_u, impurity radiation f_α, and upstream heat flux density $q_{\parallel,u}$. C_0 is defined as

$$C_0 = 7^{-2/7} (2\kappa_1)^{-3/14} \left[\int_{T_c}^{T_u} T^{1/2} L_\alpha(T) \mathrm{d}T \right]^{-1/2}, \tag{7}$$

[4] The assumed constant electron pressure stems from the assumptions that the degree of equipartition does not change, and that the modelled region lies above regions of strong ionisation and convection. Electron pressure is also affected by total flux expansion, but that effect is ignored for the purposes of this study.

and is invariant given κ_1 remains constant, and that $L_\alpha(T)$ is not cut off by the temperature limits of the detachment front. From equation (6), one can see a clear relationship between detachment front position, detachment control parameters, and divertor configuration. We can make this relationship even more apparent by expressing

$$\left[\int_{s_{\parallel,f}}^{L_\parallel} \frac{B}{B_u} \mathrm{d}s_\parallel \right]^{-2/7} = B_u^{2/7} L_{\parallel,f}^{-2/7} \langle B \rangle_{\text{above } f}^{-2/7}, \tag{8}$$

where $L_{\parallel,f} = L_\parallel - s_{\parallel,f}$ is the parallel distance between the front and upstream, and

$$\langle B \rangle_{\text{above } f} = \frac{1}{L_{\parallel,f}} \int_{s_f}^{L_\parallel} B \, \mathrm{d}s_\parallel. \tag{9}$$

Substituting equation (8) into equation (6) gives

$$C(s_{\parallel,f}) = C_0 L_{\parallel,f}^{-2/7} \frac{B_f}{B_u} \frac{B_u^{2/7}}{\langle B \rangle_{\text{above } f}^{2/7}}. \tag{10}$$

Here it should be clear to see that the control parameter required for a detachment front at position $s_{\parallel,f}$ depends on front position and divertor geometry through three terms: $L_{\parallel,f}$, $\frac{B_f}{B_u}$, and $\frac{B_u^{2/7}}{\langle B \rangle_{\text{above } f}^{2/7}}$. In subsequent sections, how these terms affect detachment access and evolution will be studied, and the predictions made will be compared against SOLPS-ITER simulations.

3. SOLPS-ITER simulations

3.1. Simulation setup

In addition to the DLS model, in this study we also use numerical plasma simulations to investigate detachment access and evolution. In particular, while the DLS model makes simple predictions about the effects of divertor geometry, simulations can be used to test these simple predictions with much more physics processes included as well as 2D effects. The SOLPS-ITER simulations used for this study are of a deuterium plasma in isolated divertor legs in idealised geometry [17], and do not include drifts or currents. An example of such an idealised geometry simulation is shown in figure 1. The benefit of using isolated divertor simulations is an enhanced ability to isolate study certain divertor features, since it is trivial to change one or two geometric characteristics of these grids at a time. These isolated geometries are created using standalone Matlab routines, satisfying a zero divergence of total magnetic field. Unless stated, the wall surfaces, target, and pump are wrapped tight around the plasma grid. The pump is located to the outer side of the target, with a length of 0.1 m. For all runs the target recycling fraction was set to 100%, and the pumping fraction was set to 5%.

For the purposes of studying detachment, the upstream electron density at the separatrix and the heat flux density into the separatrix are fixed as boundary conditions. The radial profile of these quantities can be seen in figures 1(*b*) and (*c*), and are set using the same method used in [17]. Impurities are

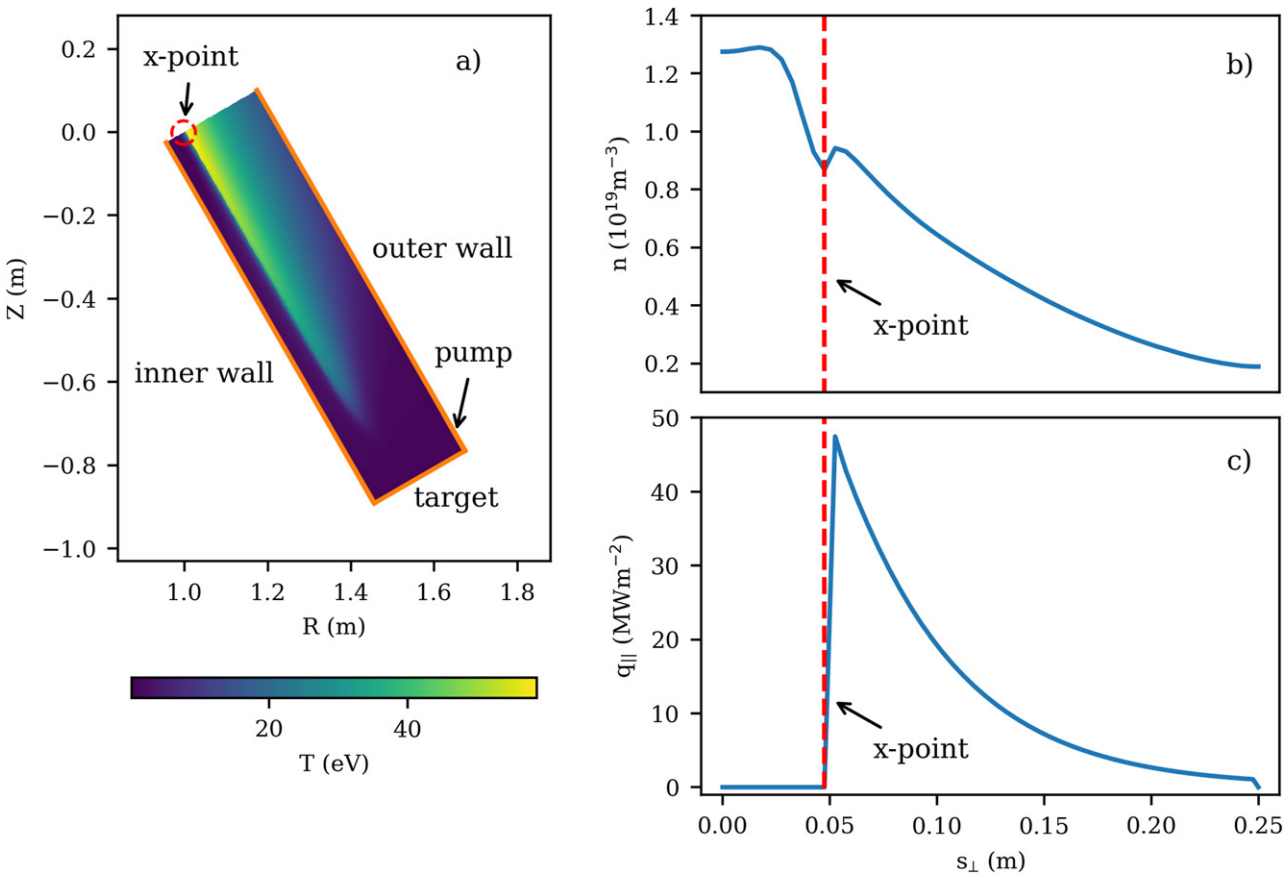

Figure 1. (*a*) A diagram of an isolated divertor leg at 30° to the vertical. A heat map of the electron temperature for a detached SOLPS-ITER simulation of this geometry is superimposed on the diagram. (*b*) An electron density profile for the simulation in (*a*) at the top of the grid, plotted as a function of radial distance from the inner edge at the divertor entrance. (*c*) A conducted electron heat flux density profile for the simulation in (*a*) at the top of the grid, plotted as a function of radial distance from the inner edge at the divertor entrance.

modelled in the divertor by having a fixed fraction of artificial impurities with the electron cooling function given by an analytical approximation for non-coronal nitrogen with $n_e\tau = 10^{20}$ m^{-3} ms (appendix A). Either the upstream separatrix electron density, upstream separatrix heat flux density, or impurity fraction can be changed across simulations to achieve a detached state. In a given converged detached state, the lumped control parameter can be post-calculated from n_u, $q_{||,u}$ and f_α. The SOL ring used for these calculations, however, is not the separatrix and instead should be roughly where the target heat flux peaks, in order to study the leading edge of a detachment front. For consistency between SOLPS-ITER runs, we do not determine the SOL ring with the maximum heat flux at the target every time, but rather use the 3rd SOL ring from the separatrix (roughly the average SOL ring where target heat flux peaks for all runs).

3.2. Detachment location in simulations

In contrast to the DLS model, determining a detachment front location in either simulation or experiment is far from trivial. This is in part because detachment is associated with a number of overlapping physical phenomena, including power loss, pressure loss, low temperatures, and volumetric recombination [10]. As such, the definition of the location of detachment can depend on which aspect of detachment is the most crucial, or easy to measure for a given study. The DLS model focuses on the power loss aspect of detachment, and defines the detachment front as the location at which all power loss occurs, beyond which there is no $q_{||}$. Even when using this specific definition, however, the front location is not obvious in simulations, since here power loss occurs continuously throughout the entire divertor. Thus we propose an analogue definition in SOLPS-ITER simulations, defining the location of detachment as the region in which *most* of the conducted heat loss occurs. Quantitatively, this means we define the front region as the narrowest physical region to contain more than 50% of loss in $\left(\frac{q_{||}}{B}\right)$. An example of such a front region, determined for a detached vertical divertor leg, is shown in figure 2.

As well as having a region for the detachment front, it is also convenient to have a single point that can denote the location of detachment. Thus we take the peak in $\frac{\mathrm{d}}{\mathrm{d}s_{||}}\left(\frac{q_{||}}{B}\right)$ as the front location, with error bars spanning the range of the 50% power loss window defined previously. Although it is not guaranteed that this location will lie in the 50% power loss window, it does for all simulations in this study. As part of this study, this definition of the detachment front was compared to several other definitions related to various aspects of detachment, and

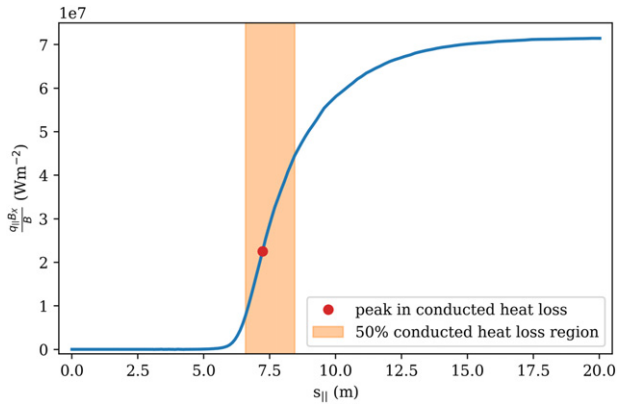

Figure 2. The electron conducted heat flux profile, accounting for magnetic field effects, plotted as a function of parallel distance from the target for a SOLPS-ITER simulation of a detached horizontal divertor leg. The narrowest window containing more than 50% of the drop in this heat flux is denoted by the orange region, and the peak in electron conducted heat flux loss is indicated by the red point.

it was found the range spanned by the 50% power loss window generally encompasses the other definitions of a detachment front (appendix B).

4. The threshold of detachment

When optimising a divertor for detachment, one of the most crucial quantities to consider is the detachment threshold, C_t. This quantity is defined as the minimum control parameter or parameter combination required for a divertor plasma to detach for a given selection of the magnetic geometry characteristics. Generally, the detachment threshold is desired to be as low as possible, to allow for easy access to detachment. Additionally, it has been shown in [1] that the upper limit of detachment control parameters (where the front reaches the x-point) is generally unaffected by the characteristics of the divertor region. Thus, with a constant upper limit, the detachment threshold defines not only the lower limit of control parameters to achieve detachment, but the effective operational window as well. In the context of the DLS model, the threshold C_t corresponds to the combination of control parameters for the detachment front colder end to be located at the target (hence the subscript 't'), and for most divertors the upstream entrance of the divertor is at the x-point. Thus, one can insert $s_{\parallel,f} = s_{\parallel,t} = 0$ and $B_u = B_X$ into equation (10) to obtain the following expression for detachment threshold:

$$C_t = C_0 L_{\parallel}^{-2/7} \frac{B_t}{B_X} \frac{B_X^{2/7}}{\langle B \rangle_{\text{above } t}^{2/7}}. \tag{11}$$

The above equation indicates that the threshold of detachment for a divertor is exclusively governed by the constant C_0, and three terms relating to the magnetic configuration of the divertor. These are divertor connection length, flux expansion, and relative line-averaged magnetic field in the divertor. Over the next section each of these properties will be explored, and compared with detachment access in SOLPS-ITER simulations. To determine the detachment threshold in simulations, we perform a scan in a single control parameter. Unless otherwise stated, these scans are performed by changing impurity concentration, keeping upstream electron density and upstream total peak heat flux density fixed at 1×10^{19} m^{-3} and 50 MW m^{-2} respectively; values representative of typical values expected in MAST-U [18]. The rough geometric features of these simulations are also similar to the range one might find in a machine similar to MAST-U, with major radii spanning from 0.5 m to 2 m, and peak magnetic fields of ≈0.5 T. The detachment front location and edges are determined for each run, and the divertor is detached when the downstream limit of the detachment front is off the target. The threshold is taken to be in the last attached simulation, with the error in threshold given by the difference in control parameter between the last attached and first detached simulations. If any values of control parameter are plotted relative to the threshold for a given geometry, the error in threshold is propagated to these values.

4.1. The role of connection length

According to equation (11), one of the key ways in which a divertor magnetic configuration can influence the detachment threshold is through the connection length (in this treatment, the parallel length of the divertor). This characteristic is present in the term $L_{\parallel}^{-2/7}$ in equation (11), and implies that obtaining a longer connection length for a flux tube will weakly decrease the detachment threshold. This term fundamentally arises through the modification of the upstream temperature; a larger $L_{\parallel}$ divertor will have a higher upstream temperature than a shorter divertor with the same $q_{\parallel,u}$ at the threshold of detachment. For the same upstream electron density, therefore, this higher temperature leads to a higher upstream pressure, which produces a higher electron density in the radiating region (typically around 5 eV for the cooling function considered here). This higher density in the radiating region means a longer divertor naturally radiates more, and consequently longer divertors are easier to detach.

To investigate the isolated effects of connection length, five vertical box grids have been generated with different physical lengths, ranging from 0.75 m to 1.5 m in the poloidal plane, and a constant $\frac{B_{\text{pol}}}{B_{\text{tor}}} = 0.05$. These grids are shown in figure 3(a), with each grid given a label from I-1 to I-4. The detachment thresholds were determined by SOLPS-ITER impurity scans for each grid [19], and are plotted in figure 3(b) as a function of connection length. These thresholds are plotted relative to the threshold determined for box I-1, since for this analysis the absolute value of detachment thresholds is less important than how they change across grids. According to the DLS model, because only the $L_{\parallel}$ term changes across these grids, the detachment threshold should vary with $L_{\parallel}^{-2/7}$. This predicted $L_{\parallel}^{-2/7}$ variation is plotted in red in figure 3(b).

Focussing first on the SOLPS-ITER thresholds in figure 3(b), we indeed see that increasing the connection length of a divertor noticeably decreases the threshold of detachment. Comparing these results to theory, however, shows that the relationship determined from SOLPS-ITER is much stronger than DLS predictions. In fact, while theory

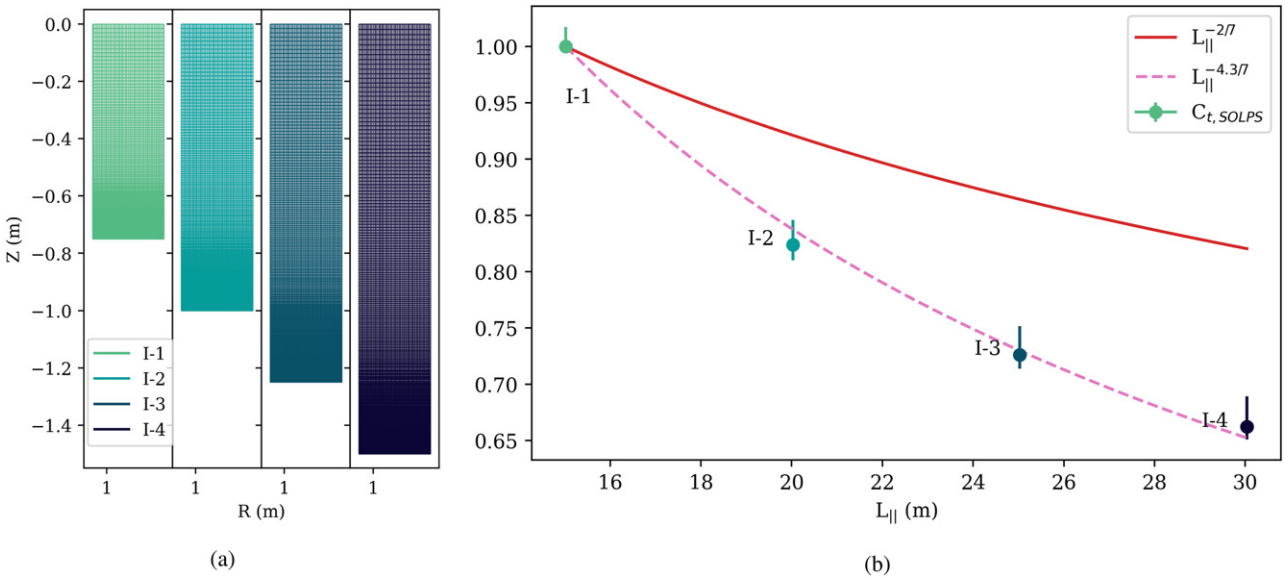

Figure 3. (*a*) The poloidal cross-sections of four vertical box divertor grids with varying connection lengths. (*b*) The SOLPS-ITER-determined detachment thresholds, connection length to the power −2/7, and a best fit polynomial for the simulated detachment thresholds for each of the five grids, normalised to the value in case I-1. Parameters are plotted as a function of connection length.

predicts a factor 1.2 lowering in detachment threshold for a doubling in connection length, the simulated results show a factor 1.7 decrease. This simulated relationship is much more aligned with a $L_{||}^{-4/7}$ relationship, as shown by the best fit curve in figure 3(*b*), and indicates there must be important physics in simulation which is not taken into account in the DLS model. In terms of designing advanced divertors, these results indicate that lengthening a divertor can be a powerful way to aid in accessing detachment—even more powerful than theory may suggest.

4.2. The role of total flux expansion

The second key way in which divertor geometry can influence detachment access is through the total flux expansion of the divertor, $F_R = \frac{B_X}{B_t}$. According to the $\frac{B_t}{B_X}$ term in equation (11), increasing total flux expansion can act to reduce the threshold of detachment. This increase in flux expansion can be achieved primarily through lowering the target magnetic field, by having a long horizontal divertor, for example. Physically, this total flux expansion term comes about because without a sink for energy, then what is truly conserved is parallel energy flux, not parallel energy flux density $q_{||}$. Consequently at a lower magnetic field where the cross-sectional area of a flux tube is greater, the instantaneous heat flux *density* will naturally be lower. As a consequence, C_t, the combination of control parameters at the target required to dissipate this lower heat flux, will also be lower.

To illustrate the effect of total flux expansion, four isolated box divertor legs at varying angles to the vertical have been generated, similar to those generated by Moulton *et al* [17], and are shown in figure 4(*a*). The total magnetic field profile in these cases is approximated to have a $1/R$ dependence, with a constant pitch angle throughout the grid. Because of the $1/R$ dependence, the total magnetic field at the target is different for each of the rotated cases. The connection length is kept the same by keeping a constant grid size and a fixed $\frac{B_{\rm pol}}{B_{\rm tor}} = 0.05$. For each of these grids, SOLPS-ITER impurity fraction scans were performed, and the determined detachment thresholds are plotted in figure 4(*b*). The theoretical thresholds for the same SOL ring were calculated using equation (11), and are also shown in figure 4(*b*). It is important to note that when these boxes are rotated, the term $\langle B \rangle_{\text{above } t}^{-2/7}$ changes in addition to total flux expansion. Thus, both this average magnetic field and total flux expansion contribution to the theoretical detachment thresholds are plotted in figure 4(*b*).

From figure 4(*b*) one can see that increasing total flux expansion (or decreasing target magnetic field) acts to significantly decrease the detachment threshold of a divertor. This conclusion has been studied theoretically before [1], and has been experimentally investigated in machines such as TCV [20, 21]. Moreover, similar to the simulated effects of connection length, we find that the simulated difference in detachment access is much stronger than theoretical predictions. In particular, DLS theory predicts moving from II-1 to II-4 should result in a factor 1.7 increase in threshold, whereas SOLPS-ITER results show a factor 2.4 increase for the same range. Although this again indicates some missing physics in the DLS model, these simulated results tend to support advanced divertors such as the MAST-U Super-X, which has a long horizontal divertor leg and a high total flux expansion [18].

4.3. The role of average magnetic field

The final divertor characteristic predicted by the DLS model to influence detachment thresholds is the divertor-averaged magnetic field. This appears as the $\frac{B_X^{2/7}}{\langle B \rangle_{\text{above } t}^{2/7}}$ term in equation (10), and implies that a higher average magnetic field in the divertor relative to that at the *x*-point will lead to a lower detachment

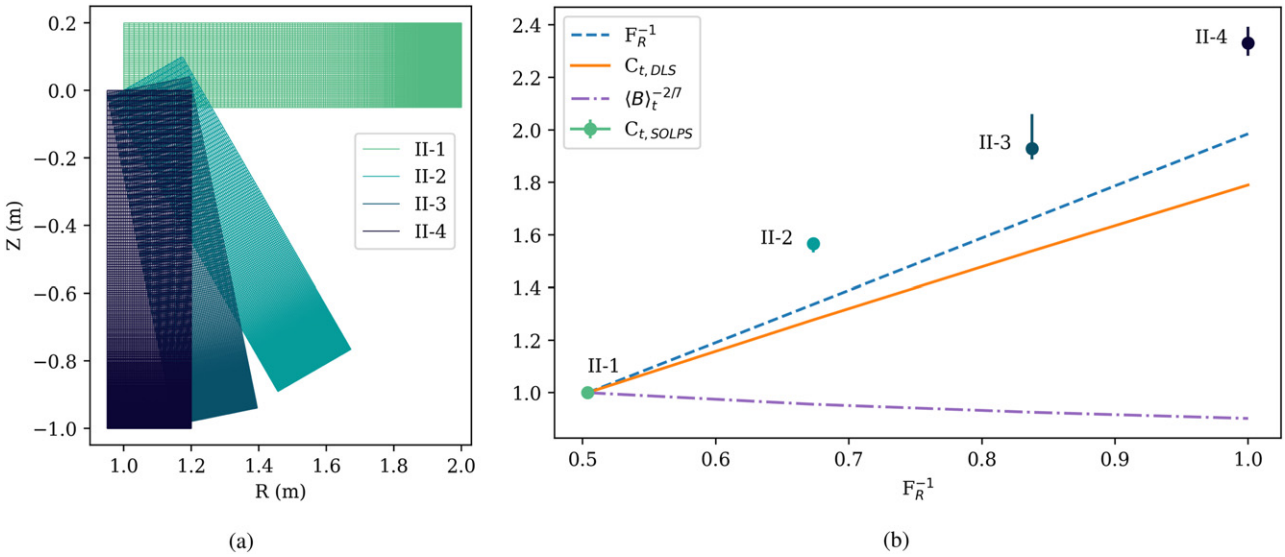

Figure 4. (*a*) The poloidal cross-sections of four box divertor grids at varying angles to the vertical. (*b*) The simulated and DLS model detachment thresholds, total flux expansion to the power −1, and divertor-averaged magnetic field to the power −2/7 for each of the four grids, normalised to the value in case II-1. Values are plotted as a function of the inverse of total flux expansion.

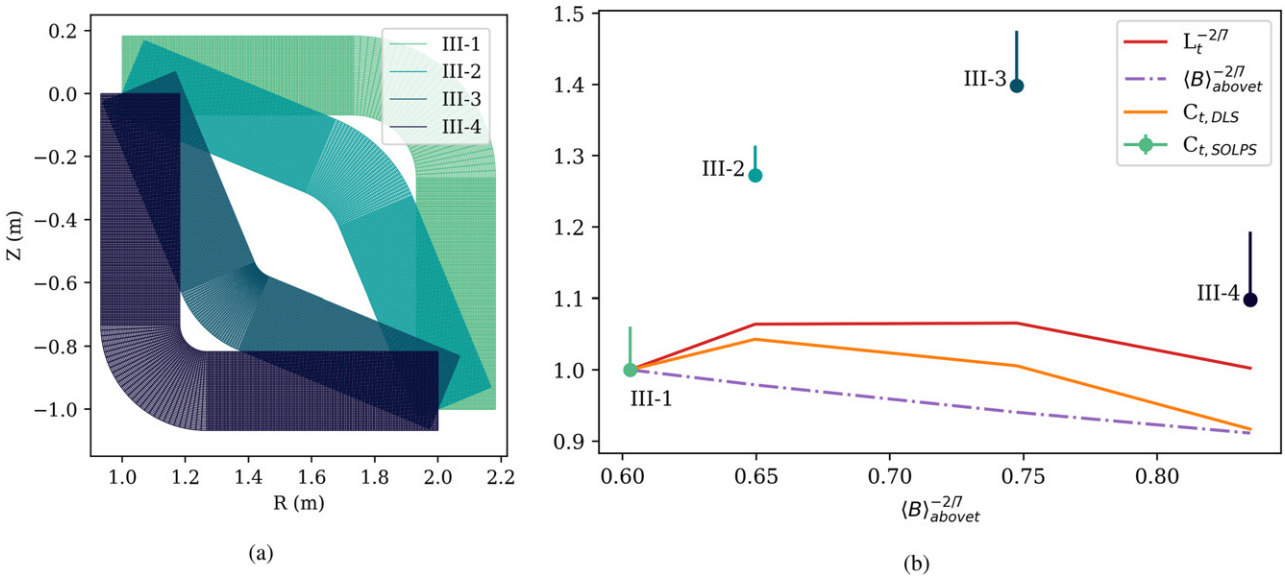

Figure 5. (*a*) The poloidal cross-sections of four kinked box divertor grids with various divertor shapes; all with the same B_x/B_t at the third SOL ring from the separatrix. (*b*) The detachment threshold, connection length to the −2/7, averaged field to the −2/7, and the DLS predicted detachment threshold for each of the four grids, normalised to their values for case III-1. Values are plotted as a function of average divertor magnetic field strength.

threshold. Similar to the effect of divertor length, this averaged field term also affects the upstream pressure through upstream temperature. This is because, given a constant target temperature, the upstream temperature is a function of the heat flux density integrated over the entire parallel distance, $L_\parallel$. While the $L_\parallel$ term affects this integrated parallel distance, the average magnetic field affects the average heat flux density within this integration region. A higher magnetic field in the divertor means a higher averaged heat flux density, and thus a higher upstream temperature at the threshold of detachment.

To demonstrate the effect of $\langle B \rangle_{\text{above } t}$ more clearly, four 'kinked' grids have been created that have the same total flux expansion at the third SOL ring from the separatrix, but the divertor leg utilizes different paths from the target to the *x*-point. These different paths are plotted in figure 5(*a*), and result in different values of $\langle B \rangle_{\text{above } t}$. In particular, the grid pairs III-1 and III-4, in addition to III-2 and II-3, have the same connection length but different $\langle B \rangle_{\text{above } t}$. The DLS model was applied to the third SOL ring from the separatrix for each of these grids, and the theoretical thresholds, connection lengths, and values of $\langle B \rangle_{\text{above } t}$ for each grid are plotted in figure 5(*b*). Additionally, the detachment thresholds for the grids were determined through SOLPS-ITER impurity scans with $n_u = 5 \times 10^{18}$ m^{-3} and $q_{\parallel,u} = 20$ MW m^{-2}, and the results are

plotted in figure 5(*b*). The reason different starting parameters were used here was to achieve converged detached states easier.

From figure 5(*b*) we see that, unsurprisingly, the DLS model predicts the detachment threshold of grid III-4 should be less than that of III-1. This is shown by the decrease of the curve $C_{t,\mathrm{DLS}}$ in figure 5(*b*), and is a direct consequence of the change in averaged magnetic field (shown by the curve labelled $\langle B\rangle^{-2/7}_{\mathrm{above}\,t}$). Similarly, the DLS model predicts a slightly better detachment access in III-3 relative to III-2. These differences, however, are small (roughly 5%–10%), and may not be noticeable if such changes were made to a real divertor. In fact, comparing the model predictions with SOLPS-ITER, we do not observe any noticeable decrease in detachment threshold as the divertor averaged field increases; in fact, we see an increase in $C_{t,\mathrm{SOLPS}}$ comparing case III-1 to III-4 and III-2 to III-3. Moreover, what small changes there may be in detachment access due to averaged field are eclipsed by the effect of connection length when comparing grids III-1 to III-2, for example. Thus, although the DLS model predicts that divertor averaged magnetic field may be important for optimising detachment, in reality the impact of $\langle B\rangle_{\mathrm{above}\,t}$ on the detachment threshold was found to be less relevant with respect to the other parameters.

The stark contrast between simulation and model results for these kinked grids may be due to the 2D transport or neutral effects. For example, although grids III-1 and III-4 have the same connection length and flux expansion at the third SOL ring from the separatrix, this is not true for the other SOL rings. In fact, farther into the SOL, the rings in III-1 will have a longer connection length and lower target magnetic field than grid III-4. This may lead to a higher density and lower heat flux density at the target in these rings, making the divertor as a whole easier to detach than expected. Similarly, because of the tight baffling around these grids, when the geometries are kinked to different angles we expect this may change the neutral trapping in addition to changes in $\langle B\rangle_{\mathrm{above}\,t}$. Specifically, in the more sharply kinked grids III-1 and III-4 one would expect more neutral trapping, which may partly explain why these grids have significantly lower thresholds relative to III-2 and III-3 than expected. Finally, the increased dependence of C_t on $L_\parallel$ determined in section 4.1 can also partly explain this large difference in thresholds.

5. The location sensitivity of detachment

It should be clear from the previous sections that there are myriad good reasons for reducing the detachment threshold in n_u, $f_\alpha^{1/2}$ and $q_{\parallel,u}^{-5/7}$, equivalent to enlarging the detachment window. Lowered detachment threshold aids in access to detachment at more reactor-like conditions than today's tokamaks—higher $q_{\parallel,u}$, lower collisionality (optimal for current drive) and, ideally, lower impurity fractions (f_α).

Of similar importance to minimizing the tokamak detachment threshold is the control of the location of detachment. Improved detachment control would allow researchers to hold a detachment front at any location from target to *x*-point, enabling studies of the effect of detachment location on both divertor and core plasma characteristics. Additionally, there is potential to design the divertor of a reactor for an expected detachment front location, adding additional armour to components surrounding the expected radiation front. Because of this, understanding how detachment fronts move as control parameters are changed may be important for achieving and maintaining an optimally detached state.

In order to understand how a detachment front location responds to a change in control parameter, we can use a quantity introduced in [1] known as the location sensitivity of detachment. The location sensitivity of detachment is defined as the differential change in front location for a given differential change in control parameter(s). An analytical form for DLS can be determined by taking the derivative of C in equation (10) with respect to $s_{\parallel,f}$, then inverting the result. This analytical form is then given by:

$$\frac{\mathrm{d}s_{\parallel,f}}{\mathrm{d}C} = \frac{1}{C}\left(\frac{1}{B_f}\frac{\mathrm{d}B_f}{\mathrm{d}s_{\parallel,f}} + \frac{2}{7}\frac{1}{L_{\parallel,f}} - \frac{2}{7}\frac{1}{\langle B\rangle_{\mathrm{above}\,f}}\frac{\mathrm{d}\langle B\rangle_{\mathrm{above}\,f}}{\mathrm{d}s_{\parallel,f}}\right)^{-1}, \tag{12}$$

where the second term on the right-hand side has been determined by realising $\frac{\mathrm{d}L_{\parallel,f}}{\mathrm{d}s_{\parallel,f}} = -1$. It is important to note that equation (12) describes the location sensitivity of a detachment front in parallel distance along a flux bundle (with respect to $s_{\parallel,f}$). In experiment, or just visualizing the detachment location in the divertor 2D cross-section, one would also want to know the location sensitivity in the poloidal plane. That information would more easily communicate the nearness to structures (for example for recycling and radiation loading) and how well the detachment front can be controlled across the divertor. We thus also derive the location sensitivity with respect to poloidal distance along a flux surface from the target, $s_{f,\mathrm{pol}}$. This poloidal sensitivity can be calculated by simply transforming $\mathrm{d}s_{\parallel,f}$ to $\mathrm{d}s_{\mathrm{pol},f}$ using $\mathrm{d}s_{\mathrm{pol}} = \mathrm{d}s_\parallel\frac{B_{\mathrm{pol}}}{B}$. The poloidal sensitivity from such a transformation is then:

$$\frac{\mathrm{d}s_{\mathrm{pol},f}}{\mathrm{d}C} = \frac{1}{C}\left(\frac{1}{B_f}\frac{\mathrm{d}B_f}{\mathrm{d}s_{\mathrm{pol},f}} + \frac{2}{7}\frac{1}{L_{\parallel,f}}\frac{B_f}{B_{\mathrm{pol},f}} - \frac{2}{7}\frac{1}{\langle B\rangle_{\mathrm{above}\,f}}\frac{\mathrm{d}\langle B\rangle_{\mathrm{above}\,f}}{\mathrm{d}s_{\mathrm{pol},f}}\right)^{-1}. \tag{13}$$

From the sensitivity equations above, it is clear there are a number of geometry-related terms that can influence the location sensitivity of detachment. In the following sections several of the terms in equation (13) will be investigated to characterise how experimentalists and divertor designers could slow down or speed up front movement for a given change in C using the magnetic characteristics of a divertor. These characteristics include local total magnetic field gradients and magnetic pitch angle. In the absence of any unique characteristics,

we shall see that as divertors become more detached, absolute location sensitivity naturally decreases.

5.1. The role of total magnetic field gradients

Upon inspection of equation (13), it is clear that a spatially varying magnetic field profile can affect detachment evolution in a divertor. This can be seen through the terms containing $\frac{\mathrm{d}B_f}{\mathrm{d}s_{\mathrm{pol},f}}$ and $\frac{\mathrm{d}\langle B\rangle_{\mathrm{above}\ f}}{\mathrm{d}s_{\mathrm{pol},f}}$. However, one would expect the contribution of $\frac{\mathrm{d}\langle B\rangle_{\mathrm{above}\ f}}{\mathrm{d}s_{\mathrm{pol},f}}$ to be small, both due to the averaged nature of this term and the factor of 2/7. Thus, we focus on total magnetic field affects only through $\frac{1}{B_f}\frac{\mathrm{d}B_f}{\mathrm{d}s_{\mathrm{pol},f}}$, which is the total (fractional) magnetic field gradient at a given location. According to equation (13), having a divertor region with a high magnetic field gradient will lower the detachment sensitivity in that region, making it harder for the front to move in response to a given change in control parameters. This term arises physically for the same reasons that flux expansion impacts the detachment threshold, discussed in section 4.2. Moving to a higher magnetic field corresponds to a higher heat flux density $q_\parallel$, and thus a higher C in order to dissipate the higher $q_\parallel$. A high magnetic field gradient, therefore, means that B_f increases significantly if a front were to change its position, and as a result C must also significantly change if the front is to move.

To demonstrate the effect of magnetic field gradients on DLS, the horizontal (II-1) and vertical (II-4) box grids from section 4.2 were investigated further. These two grids were chosen because of their contrasting magnetic field profiles. In particular, grid II-4 has no magnetic field variation, whereas grid II-1 has strong magnetic field variation throughout the entire divertor. According to the DLS model, the evolution of detachment in the horizontal box should be much less sensitive due to the presence of magnetic field gradients. To test this prediction, the SOLPS-ITER impurity scans used in section 4.2 were pushed further into more deeply detached states, until the simulations were no longer able to converge. The front positions and control parameters for the converged detached states were calculated, and are shown in figure 6(*a*), plotted relative to the detachment thresholds found in section 4.2. Such a plot of front position against control parameter will henceforth be referred to as a location evolution profile. On the same figure, the DLS predicted location evolution profiles are also plotted for each grid.

The SOLPS-ITER detachment evolution profiles in figure 6(*a*) indeed indicate a 'slowing down' in relative detachment sensitivity going from a vertical to horizontal box. Particularly at higher values of C, the horizontal SOLPS-ITER data points have a significantly lower slope than those from the vertical. For example, increasing C by 20% above its threshold value will move the detachment front by roughly 0.1 m in the horizontal grid, but more than 0.2 m in the vertical grid. Moreover, the difference in slope between the two sets of data is qualitatively similar to the difference between the horizontal and vertical predictions. Nevertheless, comparing results from each individual grid against theoretical predictions, significant deviation can be seen. Both the horizontal and vertical simulation data seems to diverge from DLS predictions, with both sets of simulation data being significantly less sensitive than theory.

When analysing the results shown in figure 6(*a*), it is very important to note that the values of C plotted are relative to the detachment threshold for each grid. Thus, the threshold needs to be taken into account to understand how a front may move with regards to some absolute value change in control parameter. To illustrate this, the same detachment evolution results in figure 6(*a*) have been plotted, but as a function of absolute control parameter $\frac{n_u\sqrt{f_\alpha}}{q_{\parallel,u}^{5/7}}$, and the results are shown in figure 6(*b*). Because these profiles are for impurity fraction scans, the x-axis of figure 6(*b*) can be thought of as a measure of the absolute value of $\sqrt{f_\alpha}$. In this plot the slope of the horizontal divertor is less steep than the vertical, though this is much less noticeable than when the relative slopes are compared in figure 6(*a*). What this means is that a given change in $\sqrt{f_\alpha}$ may result in similar front movement, since the horizontal case requires a higher percentage change in $\sqrt{f_\alpha}$, but had a lower $\sqrt{f_\alpha}$ on the threshold of detachment. Note that this is not the same for all control parameters; increasing the upstream density by a constant amount should move a detachment front significantly more in the vertical grid, since the upstream densities are identical for both grids on the threshold of detachment.

5.2. The role of magnetic pitch

In addition to magnetic field gradients, the pitch of the magnetic field at the detachment front location is predicted to have an impact on the poloidal location sensitivity, indicated by the term $\frac{2}{7}\frac{1}{L_{\parallel,f}}\frac{B_f}{B_{\mathrm{pol},f}}$ in equation (13). According to this term, increasing the ratio $\frac{B}{B_{\mathrm{pol}}}$ should lead to a decrease in poloidal location sensitivity. This is because the control parameter(s) required for a given front position depends on parallel distance, not poloidal. Thus, for a lower pitch, the same control parameter change will move the front the same distance in the parallel direction, but less in the poloidal, resulting in lower poloidal sensitivity.

To see the isolated effect of magnetic pitch angle on sensitivity, two vertical grids were generated; one completely straight, and the other with poloidal flaring at the target, both shown in figure 7(*a*). The poloidal flaring and contractions of the case labelled 'flared' leads to a varying $\frac{B}{B_{\mathrm{pol}}}$ profile, which is shown in figure 7(*b*) and contrasts with the constant profile of the 'straightdown' case. SOLPS-ITER impurity scans were performed on both grids, from attached to deeply detached states, and the control parameter and front position was recorded for each SOLPS-ITER run. The resultant position vs control parameter profiles, along with the DLS theory predictions, are shown in parallel space in figure 8(*a*) and in poloidal space in figure 8(*b*), all normalised to the threshold of detachment, C_t. It is important to note that both simulation grids have identical physical material boundaries to contain the neutrals (grey lines in figure 7(*a*)). Moreover, the SOL rings for this analysis were chosen to have the same toroidal magnetic field profiles and connection length from the target, to ensure no other geometric effects should be present.

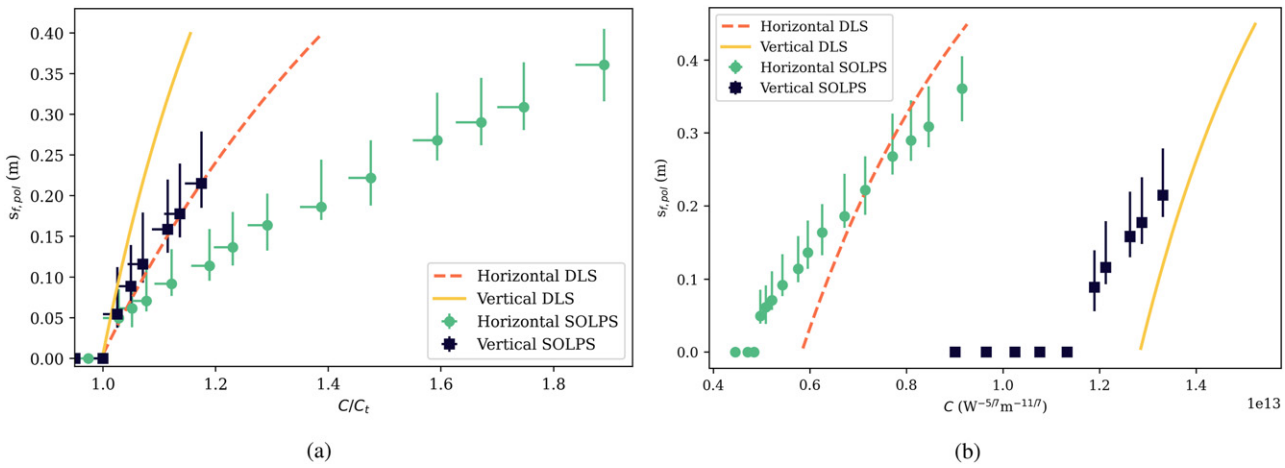

Figure 6. (*a*) The poloidal detachment front positions of grids II-1 (horizontal) and II-4 (vertical), plotted against the detachment control parameter, normalised to the SOLPS-ITER-determined threshold. The unbroken and dashed lines indicate the DLS predictions for each grid. (*b*) Identical results to (*a*), but plotted as a function of absolute control parameter C.

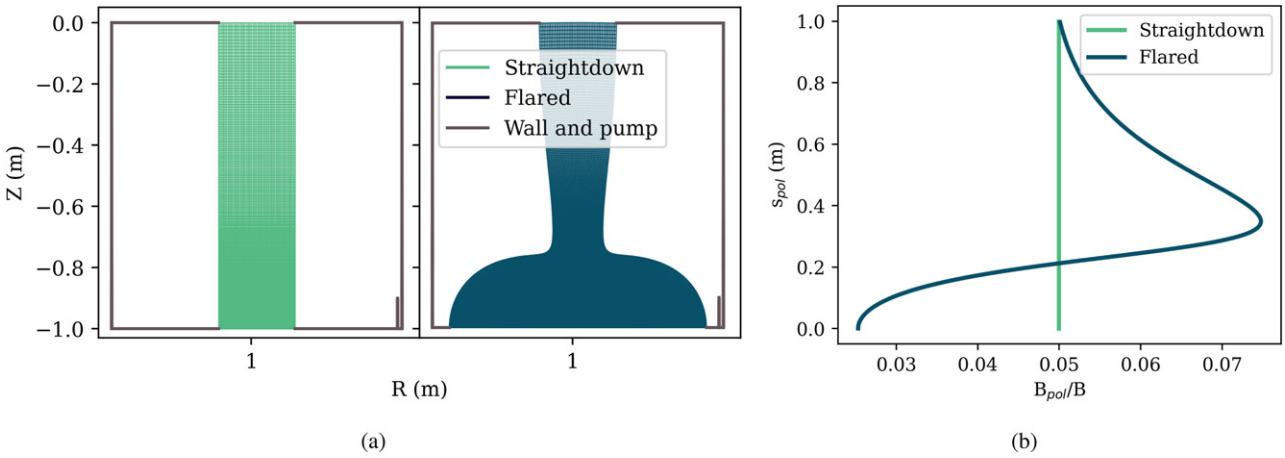

Figure 7. (*a*) The poloidal cross-sections of straight and poloidally flared vertical grids. (*b*) The magnetic pitch profile for the separatrix of the grids in (*a*).

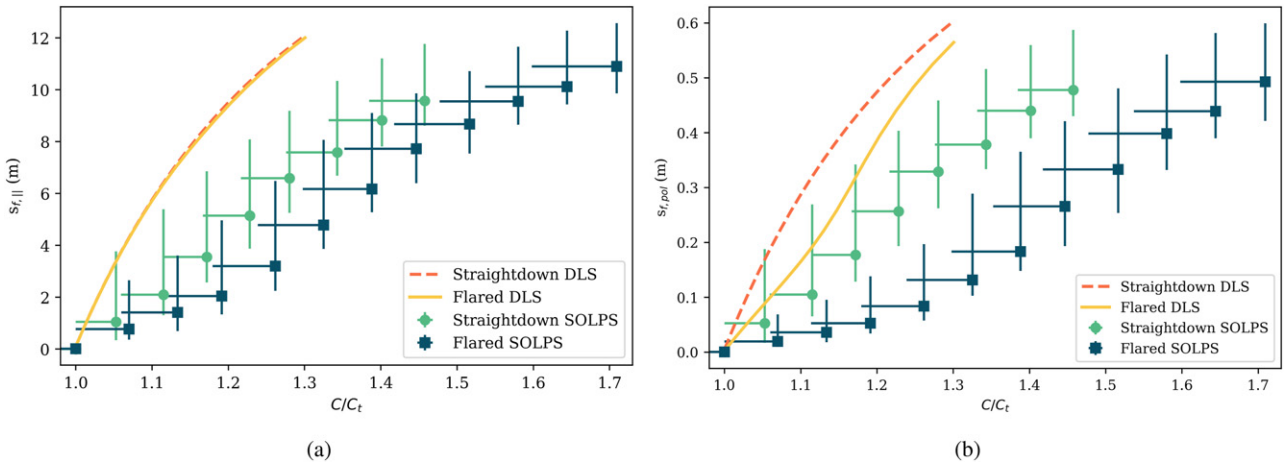

Figure 8. The (*a*) parallel and (*b*) poloidal detachment front positions for the straight and flared grids in figure 7(*a*), plotted against the detachment control parameter normalised to the SOLPS-ITER-determined threshold. DLS location evolution profiles are indicated by the unbroken and dashed lines.

Focussing first on the theoretical curves in figure 8(*a*), the DLS model clearly predicts very little change in parallel sensitivity between the straight and flared cases. This is expected, since in equation (12) there is no explicit dependence of parallel sensitivity on pitch angle. The SOLPS-ITER location evolution profiles on the same figure are similar; however, the location sensitivity is lower for the flared, compared to straightdown grid. There is also a ∼10% difference in detachment threshold despite the same connection length and flux expansion for the SOL ring considered. These differences may be attributed to 2D effects, such as the increased connection length of SOL rings further into the SOL for the flared case.

In contrast, the DLS predicted location evolution profiles in figure 8(*b*) show significantly less sensitive poloidal detachment evolution for the flared compared to the straightdown case near the target. This is of course because of the higher $\frac{B}{B_{\mathrm{pol}}}$ in this region, elongating the parallel distance travelled for a given step in poloidal distance. Comparing these predictions to simulation results, the flared case again shows much less sensitive location evolution near the target. In fact, the simulation data indicates a 30% increase in C above the detachment threshold would move a detachment front ∼0.3 m poloidally in the straightdown case, compared with ∼0.1 m in the flared case. These results may have application for advanced divertors which incorporate poloidal contraction or flaring. For example, X or Super-X divertors, which include poloidal flaring near the target may have much better control over poloidal detachment movement near the target (in addition to any increased connection length effects). Consistent with analysis presented earlier, the SOLPS-ITER results predict significantly less sensitive front movement, for a given control parameter change, than theoretical (DLS) predictions for both grids. Finally, it is important to remember that variation in pitch angle allows control over front movement only in the poloidal direction, and has little effect on parallel movement. Thus, it can be a useful tool to control how close a detachment front is to physical structures, but cannot be used to change phenomena related to parallel front position, such as variation in upstream temperature with control parameter.

5.3. The natural variation of detachment location sensitivity

To obtain a full picture of how divertors can be optimised for detachment evolution, one must also ask the question 'how does detachment naturally evolve irrespective of any manipulations of divertor geometry?'. To explore this, consider how a front might move in a divertor with no magnetic field variation and no magnetic pitch variation. In such a case equation (13) would reduce to the simple expression

$$\frac{\mathrm{d}s_{\mathrm{pol},f}}{\mathrm{d}C} \propto \frac{L_{\parallel,f}}{C}. \tag{14}$$

From this expression one can clearly see that the absolute location sensitivity naturally decreases when there is a shorter length between the front and upstream, and when the control parameter is already high. Crucially, there is generally a natural decrease in $L_{\parallel,f}$ and increase in control parameter as divertors become more detached and the front moves closer to the x-point. Thus, we can conclude that on top of any geometric effects, detachment fronts will generally become harder to move the more detached the divertor plasma is. This conclusion needs to be taken into account when considering detachment evolution, since trying to speed up front movement near the x point (by having a region of low magnetic field gradient, for example) may only slightly affect the predicted low sensitivity in this region.

Of course, when discussing how detachment fronts evolve when approaching the x-point, it is important to realise that this study considers only the divertor region and does not include regions upstream of the x-point. Because of this, the DLS model predicts zero location sensitivity as a detachment front approaches the x-point. If this model were to be applied to a topology extending to a machine's outer midplane, the sensitivity at the x-point would be much higher. Moreover, the detached SOLPS-ITER simulations for this work have generally not been pushed significantly past half way up the divertor leg. Indeed, studies of granular detachment front movement close to the x-point are sparse, and this is a topic requiring further study.

6. Detachment stability

Thus far we have explored how the variation in detachment location sensitivity from target to x-point means that better detachment location control can be had in some regions (low location sensitivity) compared to others (high location sensitivity). In addition to these regions of high and low sensitivity, divertors can theoretically have regions of negative sensitivity. Equation (13) shows that such negative sensitivity regions can be achieved with a sufficiently 'negative' magnetic field gradient, $\mathrm{d}B_f/\mathrm{d}s_{\parallel,f}$. Specifically, the condition for a negative sensitivity is given by:

$$\frac{1}{B_f}\frac{\mathrm{d}B_f}{\mathrm{d}s_{\mathrm{pol},f}} < \frac{2}{7}\frac{1}{\langle B\rangle_{\mathrm{above}\ f}}\frac{\mathrm{d}\langle B\rangle_{\mathrm{above}\ f}}{\mathrm{d}s_{\mathrm{pol},f}} - \frac{2}{7}\frac{1}{L_{\parallel,f}}\frac{B}{B_{\mathrm{pol}}}. \tag{15}$$

According to this equation, negative DLS should be apparent in a number of different divertor profiles, and in particular inner target divertors where the magnetic field at the target is greater than that at the x-point. What, however, would such a negative sensitivity mean for detachment location control for those divertor geometries? Theoretically, a negative sensitivity means that it is easier for a divertor to be in a more detached state, since it needs a lower control parameter to have a more detached front. Because of this, one would expect that if a front existed in a region of negative sensitivity, it would not exist there stably, and would instead move further and further away from the target, until it reached a stable (positive location sensitivity) point with the same control parameters. Hence, we expect regions of negative location sensitivity to correspond to unstable regions where no stable detachment front can exist.

To show this more explicitly, the DLS equations were applied to a grid at -10° to the vertical, which has a negative magnetic field gradient from the target to the x-point. This grid is shown in figure 9(*a*), and the predicted location evolution profile is shown in figure 9(*b*). Thinking about how

detachment evolves with such a profile, one may start by asking what would happen if a divertor is attached at the threshold of detachment, and C is increased slightly—to $1.01C_t$ for example. For the case shown in figure 9(*b*) the detachment front would jump to 0.5 m off the target, because this corresponds to the next stable solution satisfying the specified C. Once in this deeply detached state, one would expect well behaved movement as C is increased further, since the location evolution profile here is stable and continuous. Similarly, if a divertor were to start in a deeply detached state and C was decreased, there should be continuous movement until 0.25 m off the target, at which point decreasing C further would cause the front to reattach (since there are no detached solutions for C). Crucially, no matter which direction the front moves in, it never exists in the unstable region of negative sensitivity, which ranges from 0 to 0.25 m off the target. Perhaps just as importantly, we also note that the presence of negative sensitivity allows for a hysteresis of sorts for detachment evolution. Starting from an attached state, detachment is achieved at the threshold. Decreasing C from a detached state, however, allows detached operation even below the detachment threshold; in the case of figure 9(*a*), at $C = 0.98C_t$.

These DLS predictions for negative sensitivity could potentially be useful for real divertor geometries with negative magnetic field gradients; inner legs for example, or outer divertors with poloidal flux contraction at the target. The prediction that no detachment front should exist in regions of negative sensitivity may allow researchers to design a divertor where fronts can avoid certain disadvantageous positions. Moreover, the prediction that negative sensitivity geometries can stay detached below the detachment threshold may allow devices to operate safely near the detachment threshold, with an effective buffer zone created by the presence of negative sensitivity. Because of the potential applications of some of these conclusions, it is vital to determine whether these predictions are also observed in more complex environments such as simulation or experiment. As such, two SOLPS-ITER impurity scans were performed on the grid in figure 9(*a*); one starting from an attached state and increasing C, and the other starting from a very detached state and decreasing C. The post-calculated location evolution profiles for these scans are shown in figure 10, with values of C normalised to the threshold found by the increasing C scan.

Inspecting figure 10, many of the broad features predicted by the DLS model for regions of negative sensitivity are also present in SOLPS-ITER simulations. In particular, starting from an attached state and increasing C, a large jump in front position of 0.25 m is found just above the threshold, followed by well-behaved continuous detachment location movement as C is increased further. Furthermore, when operating in a detached state and decreasing C, detachment is retained while operating up to 8% below the detachment threshold. Finally, if C is decreased sufficiently, the front jumps back to an attached state. The most significant difference between the SOLPS-ITER and DLS model predictions for this grid is that absolute magnitude of the location sensitivity (or slope of the evolution profiles) in the SOLPS-ITER case is significantly lower than DLS predictions. This means that the region of detachment instability in the SOLPS-ITER results is much physically thinner in S_{pol} than DLS predictions, but also means that C can be reduced more below the threshold before reattaching than theory predicts.

7. Discussion

Throughout this paper features of divertor geometry affecting detachment have been studied, both using the DLS model and simplified geometry SOLPS-ITER simulations. Both tools, however, inevitably fall short of completely describing the physical complexity of detachment evolution in experiment, and the logistic complexity of divertor and machine design. Throughout the following section the utility and limitations of both the DLS model and the simulations used in this analysis will be discussed. In particular, the differences in physics processes included in SOLPS-ITER and the DLS model will be examined; to point towards what the key pieces of missing physics of the DLS model might be. The boundary conditions and included physics of the SOLPS-ITER simulations will also be discussed, highlighting key differences to be expected when moving to more complex simulations or experiment.

7.1. Limitations of the DLS model

Many of the results shown thus far have highlighted differences between predictions made by the DLS model and results calculated from SOLPS-ITER simulations. These differences indicate that there is very likely some missing detachment physics not taken into account by the DLS model. This is not surprising, given the simplicity of the DLS model; nevertheless it is still useful to highlight the key assumptions that are broken when moving to simulations, and therefore, that are expected to be broken in experiment.

The derivation of the equations of the DLS model begin with equation (1), which is simply an equation for heat balance along a SOL ring and to derive it requires no more assumptions than those present in a SOLPS-ITER simulation. To produce the final equations of the DLS model, however, three broad assumptions must be made: the assumption that the detachment front is thin in parallel space, the assumption that static electron pressure is conserved upstream of the detachment front, and the assumption that impurity radiation is the only sink for conductive electron heat flux. Throughout the following section, the validity of these assumptions will be explored, as well as their relative contribution to disagreements between the DLS model and SOLPS-ITER.

The first broad assumption made by the DLS model equations is that the front is thin, such that the variation of B across it is small and that upstream of the front $q_{\parallel} = q_{\parallel,u}\frac{B}{B_u}$. Included in this assumption is the premise that the conducted heat flux is not limited, and that the heat flux can therefore be written $q_{\parallel} = -\kappa_1 T^{5/2}\frac{\mathrm{d}T}{\mathrm{d}s_{\parallel}}$ with constant κ_1. In the SOLPS-ITER simulations, however, heat can be lost over a wide region, and a flux limiter is active with a flux limiting coefficient $\alpha = 0.3$, producing a detachment front with a finite width. As a result, there may be disagreements between the

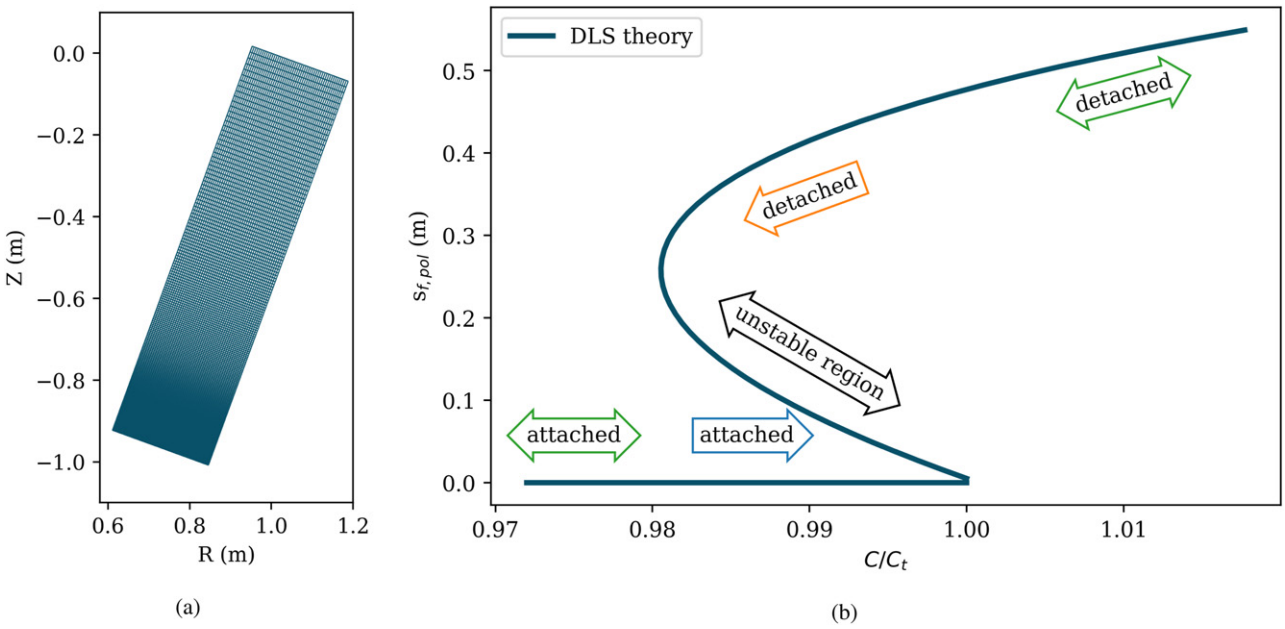

Figure 9. (*a*) A grid for an inner target divertor leg at an angle of -10° to the vertical. (*b*) The detachment location evolution profile of the third SOL ring from the separatrix in (*a*), calculated by the theoretical DLS equations. Green arrows indicate stable continuous regions, blue arrows indicate stable regimes only accessible from an attached state, orange arrows indicate stable regimes only accessible from a deeply detached state, and black arrows indicate unstable regions not accessible from either direction.

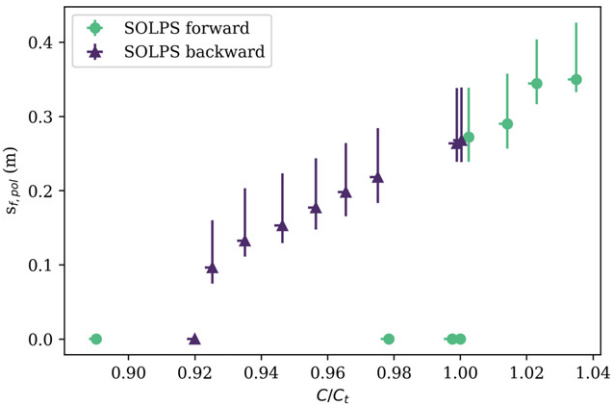

Figure 10. The detachment location evolution profile for the grid in figure 9(*a*), post-calculated from SOLPS-ITER data. The circular data points labelled 'SOLPS forward' are for an impurity fraction scan starting from an attached state and becoming more detached. The triangular data points labelled 'SOLPS backward' indicate an impurity fraction scan starting from a detached state and becoming less detached.

DLS model and SOLPS-ITER, since the effective front position at which geometric parameters such as B_f and $L_{\parallel,f}$ are evaluated may be incorrect. To evaluate how strongly the assumption of a small detachment front width is violated, the front widths were calculated for all 85 detached simulations used for this study. The widths were calculated using the 50% electron conducted heat flux loss region defined in section 3.2. The average parallel width determined for the SOLPS-ITER simulations is 2 m. Though this width is non-negligible, the average variation in total magnetic field strength across these widths is only 2%. Moreover, the effects of this non-negligible front width has been partially accounted for by the implementation of front position error bars on all detachment evolution plots.

The second key assumption of the DLS model is that of a constant electron static pressure within the detachment front. This of course is not exactly true in simulation of experiment, since the electron static pressure can be lost or gained in and above the front region, through exchanges with other pressures or through volumetric sources or sinks [22]. To illustrate this, the decomposition of total pressure for one attached and one detached SOLPS-ITER simulation is shown in figures 11(*a*) and (*b*). From these figures, it is clear to see the static electron pressure is not constant throughout the divertor, and can change by a factor 2 or more within the front region. This decrease in static pressure may be caused partially by exchanges with the ram pressure or ion–electron equipartition, but is also likely affected by other momentum sinks such as charge exchange or cross-field transport of momentum. To further quantify the assumption of constant $n_e T_e$, the electron static pressure at the front location has been calculated relative to the upstream static electron pressure for all detached simulations used for this study. The average fractional pressure at the front was determined to be 0.7 ± 0.2. This significant deviation from the expected fractional pressure of 1 shows the assumption of constant static electron pressure can be broken to a meaningful degree in these simulations. Notwithstanding, it is important to note that the overlap between the detachment front region and a region of significant pressure loss may strongly depend on the choice of impurities, and may not hold true for a higher temperature radiator such as neon.

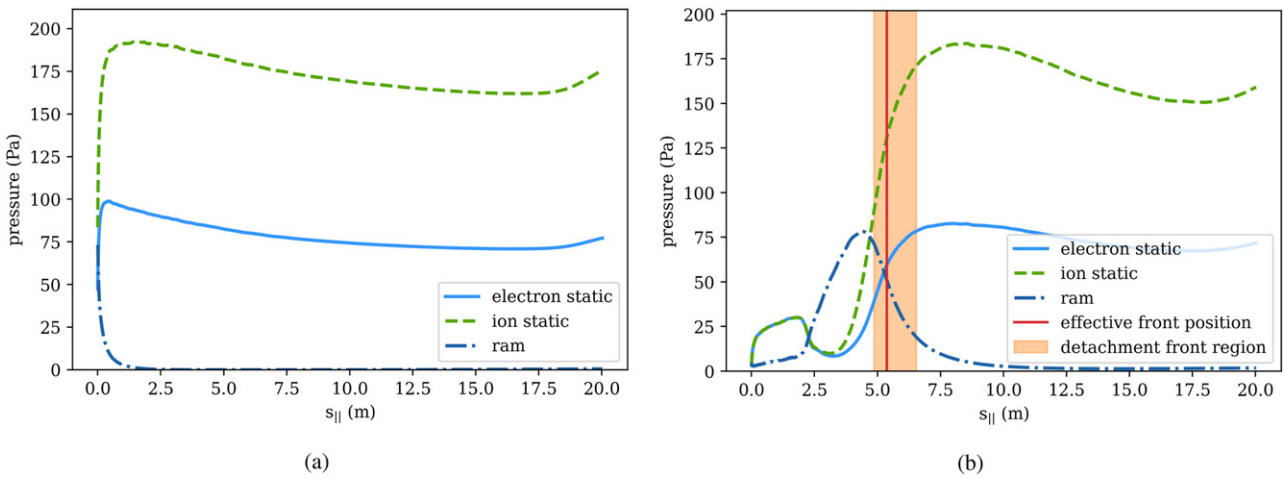

Figure 11. (*a*) The decomposition of several contributions to pressure for (*a*) an attached and (*b*) a deeply detached simulation of a horizontal divertor.

The final assumption of the DLS model is that impurity radiation is the dominant sink for the parallel electron conducted heat flux density. In reality, however, this heat flux density can be lost or gained through sources and sinks, exchanged with other channels of heat flux, and/or transferred radially between flux tubes. To illustrate this, the decomposition of total heat flux density for a attached and deeply detached simulation is plotted in figures 12(*a*) and (*b*). Additionally, several dominant power loss channels for these simulations are shown in figures 13(*a*) and (*b*). From figures 12(*a*) and (*b*) one can see that the assumption of an electron conduction plasma breaks down, since ion conduction plays a strong role upstream, and within the detachment front region the plasma becomes convection-dominated. However, the role of ion conduction in these simulations is not indicative of experiment, since the fraction of parallel power into the ion and electron channels was set to 50:50 at the divertor entrance. For future studies, this ratio should be altered, particularly to see if a higher fraction of power to the electron channel produces more favourable agreement with the DLS model.

In figure 13(*b*), it seems the assumption of an impurity-dominated power sink is valid for the detached case, but the attached simulation in figure 13(*a*) shows impurities and deuterium dissipate roughly equal amounts of power. To investigate the violation of these assumptions in more detail, the fraction of the upstream electron conducted heat flux dissipated by impurity radiation was calculated for every detached simulation used for this study. The average fractional power dissipated by impurities is 110% $\pm$ 20% (note this is greater than 100% because this is a fraction of the electron conducted heat flux, not the total). Though the average agrees with the assumed dissipation of 100%, the deviation in dissipated power between simulations could be a source of model disagreement.

From the comparative analysis presented thus far, it should be apparent that the three broad assumptions made by the DLS model to produce simple quasi-analytical equations are broken to a considerable degree in the SOLPS-ITER simulations presented. What perhaps is not as clear is how much each of these broken assumptions affect the quantitative disagreements between the DLS model and SOLPS-ITER simulations. To investigate this further, the DLS model can be applied to the simulations at four different levels of complexity. The first is the standard DLS model presented previously, using equation (6). For the second, the assumption of a thin front is removed, so that the model solves for the heat balance equation

$$\frac{q_{\parallel,u}^2}{B_u^2} = -f_\alpha n_u^2 T_u^2 \int_{s_{\parallel,c}}^{L_\parallel} \frac{2q_\parallel T^{-2} L_\alpha(T)}{B^2} \mathrm{d}s_\parallel, \tag{16}$$

using the real electron temperature profile from SOLPS-ITER. Of course, when the true SOLPS-ITER electron temperature profile is used, including the true upstream temperature, this represents more than simply removing the assumption of a thin front. However, for this simple analysis, let equation (16) represent the DLS model applied to a more realistic detachment front shape. In the third version of the model, the assumption of constant pressure can be removed, so that the model solves the equation

$$\frac{q_{\parallel,u}^2}{B_u^2} = -f_\alpha \int_{s_{\parallel,c}}^{L_\parallel} \frac{2q_\parallel n^2 L_\alpha(T)}{B^2} \mathrm{d}s_\parallel, \tag{17}$$

with the real density profile from SOLPS-ITER. Finally, the most complex version of the model solves the full equation for heat balance shown in equation (1), including all sources and sinks of heat from SOLPS-ITER, such as hydrogenic losses and gradients in other flux channels. This is the most complex model, which should match with SOLPS-ITER within numerical tolerance. By comparing the output of these four models, it should be made clear which assumptions are important for creating disagreements between the DLS model and SOLPS-ITER.

Indeed, these equations have been applied to evaluate the detachment thresholds for the 12 different geometries considered in section 4. Figures 3(*b*), 4(*b*) and 5(*b*) have been reproduced with data from these intermediate models, and are shown in figures 14(*a*)–(*c*). Inspecting these figures, when

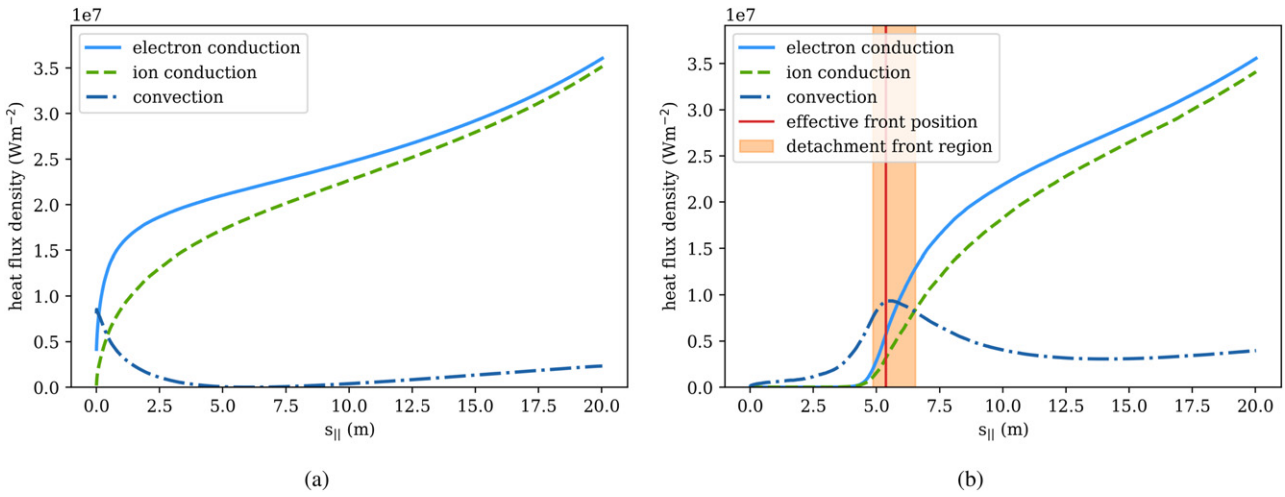

Figure 12. (*a*) The decomposition of several channels of heat flux density for (*a*) an attached and (*b*) a deeply detached simulation of a horizontal divertor.

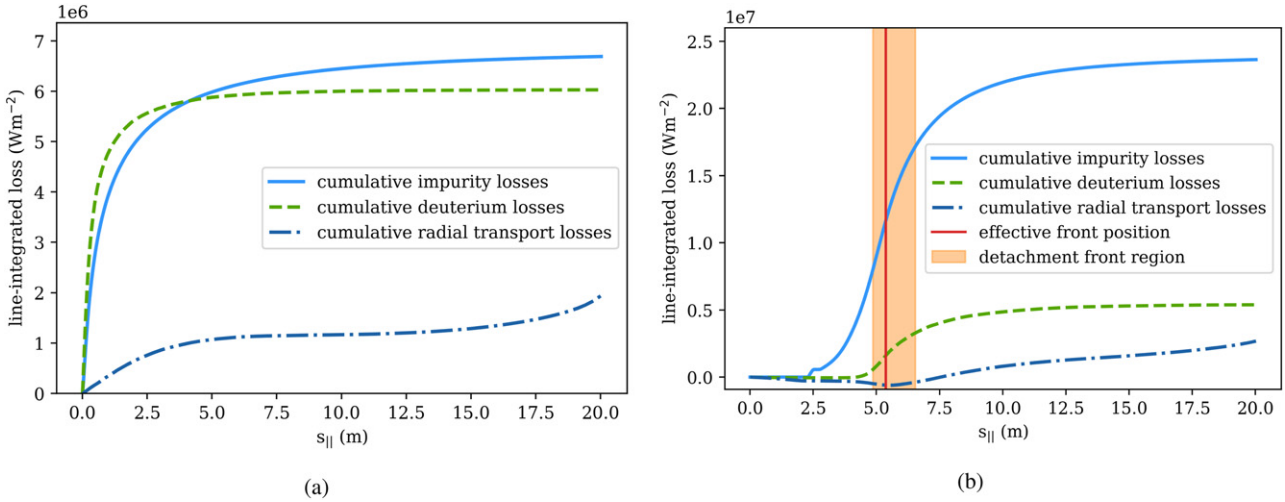

Figure 13. The decomposition of the dominant power sources and sinks (*a*) an attached and (*b*) a deeply detached simulation of a horizontal divertor. These losses are integrated cumulatively starting from the target.

equation (16) is applied to the simulations with the true temperature profile and no assumptions about front width, there is a noticeable but small difference between the simplest DLS model. Increasing in complexity again with equation (17), and using the true density profile from SOLPS-ITER with no assumptions about pressure, a very significant difference can be seen, with much better match of the predicted thresholds to SOLPS-ITER. Finally, adding the full sources and sinks to the heat balance recovers the SOLPS-ITER calculated thresholds. This final change is significant, but less so in general compared to removing the constant pressure assumption. Overall, this analysis shows that the assumption of constant pressure seems to be the leading cause of discrepancy between the DLS model predictions and the SOLPS-ITER simulation data presented in this work.

7.2. Limitations of simulations

As well as the DLS model, even the SOLPS-ITER simulations presented here are limited in their scope, and as such the conclusions presented here must be tempered with knowledge of these limitations. In particular, the simulations used have neglected the effects of drifts and currents, which have been shown to significantly alter the expected densities and temperatures at divertor targets [23]. It is difficult to say how the effects of drifts would change with divertor configuration or machine. For example, a spherical tokamak may have stronger magnetic field gradients enhancing the $\nabla B \times B$ drifts, but spherical tokamaks also typically have larger SOL widths (and therefore lower radial electric fields) which lower the strength of the $E \times B$ drifts. Additionally, radial transport coefficients

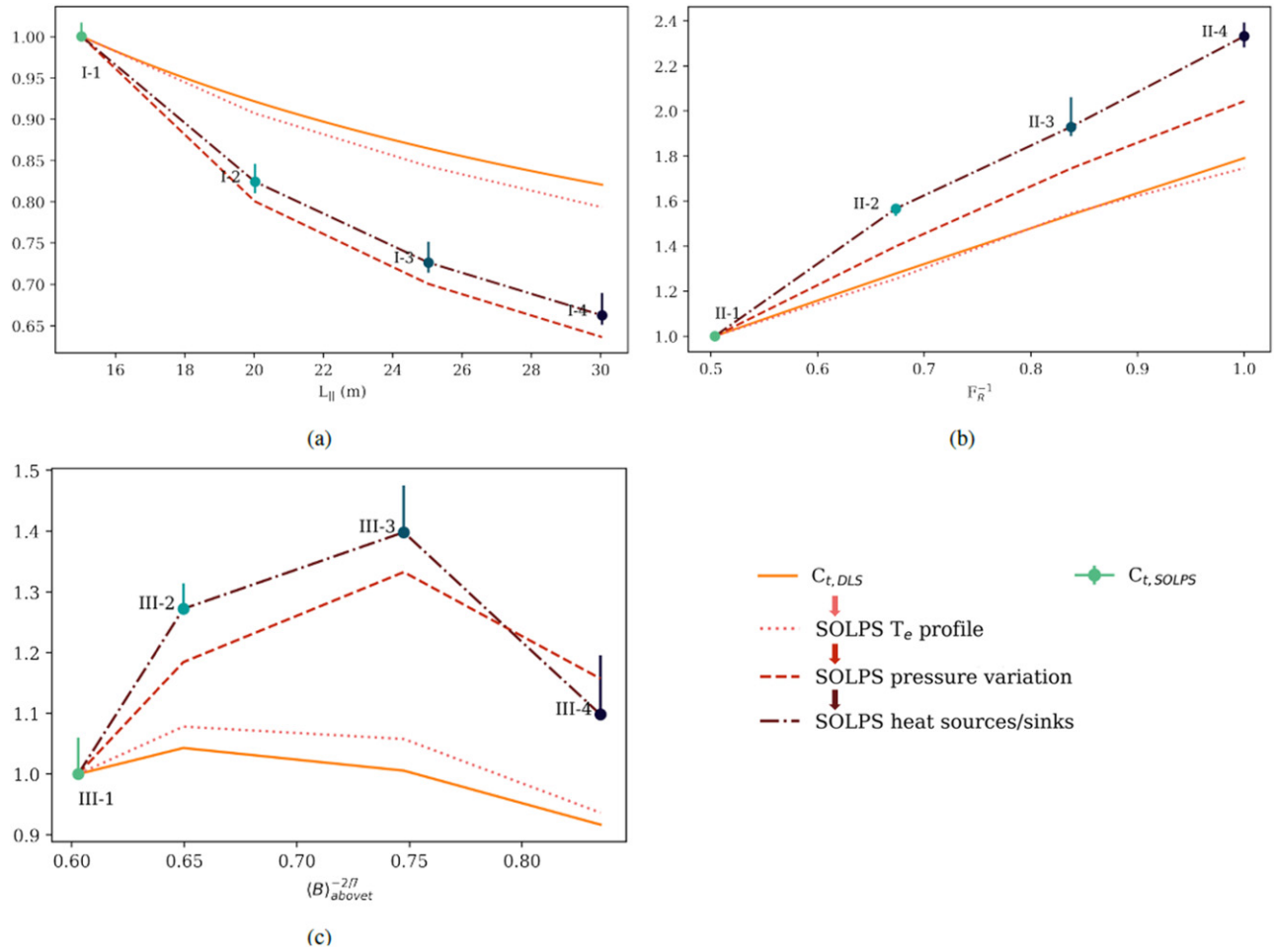

Figure 14. (*a*) The detachment thresholds for the grids in figure 3(*a*) are plotted as a function of connection length. (*b*) The detachment thresholds for the grids in figure 4(*a*) are plotted as a function of inverse total flux expansion. (*c*) The detachment thresholds for the grids in figure 5(*a*) are plotted as a function of the divertor averaged magnetic field. The thresholds are calculated using the simple DLS model (labelled $C_{t,\mathrm{DLS}}$), a version of the model which uses the true temperature data from SOLPS-ITER (labelled 'SOLPS T_e profile'), a version which also uses the true density data from SOLPS-ITER (labelled 'SOLPS pressure variation'), and a version which solves for the true heat balance in SOLPS-ITER (labelled 'SOLPS heat sources/sinks'). These models are compared to the post-calculated thresholds from SOLPS-ITER.

are set as constants throughout all SOLPS-ITER simulations, which does not fully capture turbulent radial transport and how the strength of such transport may change with magnetic configuration and detachment front position. These simulations are also run in a time-independent mode, and thus give incomplete knowledge as to how a divertor can evolve between different detached solutions. The investigation of time-dependent simulations would be very useful in future work, particularly for the negative sensitivity study shown in figure 10.

Moreover, the box simulations used for this analysis are not full-geometry simulations of real divertor configurations. Consequently, they are neglecting the effects of power sources and sinks above the *x*-point and the connection length to the midplane which can be much larger than the connection length below the *x*-point. Another additional simplification for these simulations is the incorporation of artificial radiating impurities with an impurity fraction which is constant in the entire divertor. Of course, this simplification allows for better comparison to the DLS model. However, in reality, the transport of seeded impurities and densities of different charge states is crucial for completely understanding the role of power sinks in detachment. Furthermore, apart from impurity concentration and plasma geometry, all parameters and boundary conditions in the SOLPS-ITER scans have been kept constant in all runs. These constants are of course useful for the scope of this study, but it is important to note that changing these other parameters can also significantly affect detachment. The target recycling coefficient or pumping albedo, for example, are kept constant, but have also been shown to significantly affect detached SOLPS-ITER simulations [17].

Finally, it is vital to remember that all scans in C performed in this study have been achieved through changing impurity fraction, $\sqrt{f_\alpha}$. Even though the DLS model predicts that changing n_u or $q_{||,u}^{-5/7}$ should give identical results, this is not necessarily true in either simulation or experiment. To illustrate this point, detachment evolution SOLPS-ITER scans in n_u and $q_{||,u}$ were performed for the horizontal box case (II-1) shown in figure 4(*a*). For the density scan, $q_{||,u}$ was fixed at

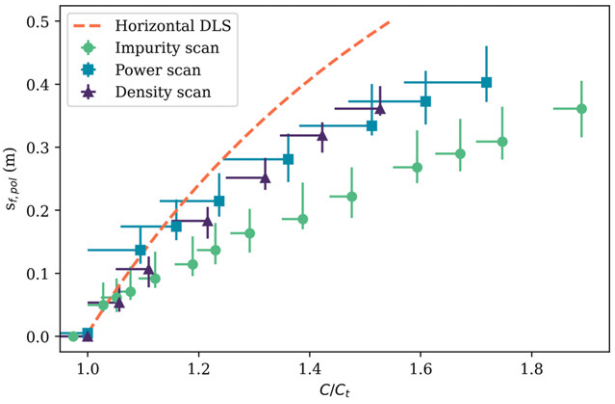

Figure 15. Detachment location evolution profiles for the third SOL ring from the separatrix in grid II-1. The circular data points are for an control parameter scan driven by impurity concentration, the square data points are for a scan in upstream power, and the triangle data points are for a scan in upstream electron density.

50 MW m^{-2}, for the power scan n_u was fixed at 10^{19} m^{-3}, and for both scans f_α was fixed at 1.7%. The results of such a scan are shown in figure 15, compared with the original impurity fraction scan and DLS predictions. These results clearly show a significant qualitative difference in location evolution profiles between the control parameters, with upstream electron density and heat flux density agreeing much more closely to theory. Thus, to obtain a complete picture of detachment evolution, one must consider detachment access and evolution dominated by changes in all control parameters, not just impurity concentration.

8. Conclusions

The DLS model is a simple yet powerful model that can be used to predict the relationship between divertor configuration characteristics and the behaviour of detachment; detachment threshold as well as the relationship between detachment location variation and control variables. When applied to study the operational window of detachment, the DLS model predicts that divertors with long connection lengths, high total flux expansion, and high average magnetic fields in the divertor will produce the largest operational window in control variables that allow the divertor to stay detached. When compared to detachment access results from SOLPS-ITER simulations of simple isolated divertor grids, the effects of total flux expansion and connection length are even more pronounced, with the averaged magnetic field seemingly having little effect on detachment access. These mathematical features can be achieved by varying engineering properties of the divertor, such as making divertors more horizontal (particularly near the target), and making divertor legs as long as possible (both physically and through lower poloidal field strength).

Additionally, the DLS model and SOLPS-ITER can also be applied to study how a detachment front moves from the target to the x-point. The model equations show that divertor configurations can have regions where a detachment front may naturally be resistant to movement, and regions where detachment fronts are prone to movement as control variables are varied. Low sensitivity regions in which fronts are not easily moved can be achieved by having high magnetic field gradients, low magnetic pitch angles, or occur naturally for deeply detached states. Furthermore, regions of negative location sensitivity can exist given a sufficiently high magnetic field gradient towards the target. No stable detachment front locations can exist in such regions; thus, if a detachment front is not desired in a particular location, the magnetic field gradient in that location could potentially be engineered to ensure that a detachment front cannot exist there. Moreover, simulations and modelling show that these regions can allow detached states below the detachment threshold, offering a buffer zone for configurations such as inner leg divertors.

Though the DLS model and SOLPS-ITER box simulations are powerful tools to study detachment, one must also be aware of their limitations to fully appreciate any conclusions drawn. The DLS model makes many simplifying assumptions concerning detachment physics, including assuming constant pressure loss, and neglecting non-impurity power sinks. Analysis seems to indicate that pressure and power sources and sinks may be a key reason behind the qualitative differences between DLS model predictions and SOLPS-ITER results. Although SOLPS-ITER simulations offer more physical complexity, they are also limited in that only impurity scans have been used in data analysis, and that only a narrow range of boundary conditions have been explored. Finally, the conclusions presented here pertain to how divertor configuration can influence the behaviour and control of detachment. To truly optimise divertors, a range of other practical and physics considerations must be made, such as the size of a machine, the space for elongating the divertor leg in major radius and the poloidal field coils available for manipulation of the divertor magnetic properties.

Acknowledgments

This work has been part-funded by the RCUK Energy Programme (Grant Number EP/T012250/1), and in part performed under the auspices of the US DoE by LLNL under Contract DE-AC52-07NA27344. This work has been carried out within the framework of the EUROfusion Consortium and has received funding from the Euratom Research and Training Programme 2014–2018 and 2019–2020 under Grant Agreement No. 633053. The views and opinions expressed herein do not necessarily reflect those of the European Commission.

Appendix A. An approximated electron cooling function for nitrogen

The SOLPS-ITER simulations used in this study incorporate impurity radiation by having some fixed fraction of artificial impurities. These impurities radiate with an analytical electron cooling function meant to approximate that of nitrogen. This analytical form is given in [1], and is an approximation for the non-coronal model for nitrogen in [24]:

$$L_N = 5.9 \times 10^{-34} \frac{(T - 1\ \text{eV})^{1/2}\,(80\ \text{eV} - T)}{1 + 3.1 \times 10^{-3}(T - 1\ \text{eV})^2}\ \text{W m}^3 \quad (18)$$

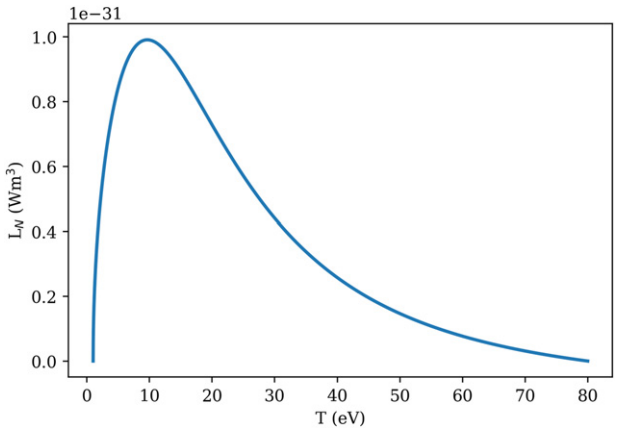

Figure 16. An analytically approximated electron cooling function for nitrogen, the form for which is given in equation (18).

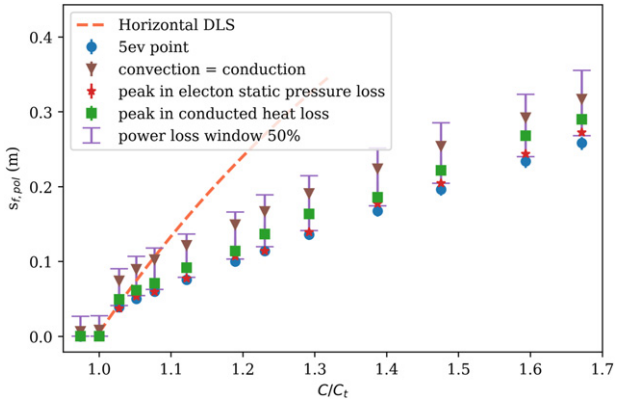

Figure 17. The SOLPS-ITER detachment location evolution profile for the third SOL ring of grid II-1, with detachment front position determined using a range of different methods. These methods are compared to DLS theory, indicated by the dashed curve.

for 1 eV $< T <$ 80 eV, and $L_N = 0$ otherwise. A plot of this cooling function is shown in figure 16 below.

Appendix B. Comparing definitions of detachment location in simulations

Based upon the various physical phenomena associated with detachment, we have investigated several methods of determining the location of a detachment front in simulation. There is of course no 'correct' definition; instead one method may be better suited for a particular study, such as comparing to models or to experiment. The methods we have formulated are:

(a) The point at which the electron temperature is 5 eV.
(b) The point at which the convected heat flux is equal to parallel electron conducted heat flux, forming the boundary between the conduction-dominated plasma and convection-dominated detached region.
(c) The local peak in electron static pressure loss, $\frac{\mathrm{d}(nT)}{\mathrm{d}s_\parallel}$.
(d) The peak in electron conducted heat loss, $\frac{\mathrm{d}}{\mathrm{d}s_\parallel}\left(\frac{q_\parallel}{B}\right)$.
(e) The narrowest physical window containing 50% of electron conducted heat loss, $\frac{q_{\parallel,\mathrm{end}}}{B_{\mathrm{end}}} - \frac{q_{\parallel,\mathrm{start}}}{B_{\mathrm{start}}} = 0.5\frac{q_{\parallel,X}}{B_X}$.

These methods have been applied to find the detachment front positions for an impurity scan in SOLPS-ITER for a horizontal box grid (geometry II-1). The location evolution profile for each of these front definitions is shown in figure 17. It is clear to see from this figure that the variation in front position between definitions is roughly encapsulated by the narrowest physical window containing 50% of electron conducted heat loss. This tends to indicate that the window containing 50% of electron conducted heat loss is an appropriate choice for the errors in front position.

ORCID iDs

C. Cowley https://orcid.org/0000-0001-7065-8922
B. Lipschultz https://orcid.org/0000-0001-5968-3684
B. Dudson https://orcid.org/0000-0002-0094-4867

References

[1] Lipschultz B., Parra F.I. and Hutchinson I.H. 2016 Sensitivity of detachment extent to magnetic configuration and external parameters *Nucl. Fusion* **56** 056007
[2] Aymar R., Barabaschi P. and Shimomura Y. 2002 The ITER design *Plasma Phys. Control. Fusion* **44** 519
[3] Federici G. *et al* 2014 Overview of EU DEMO design and R & D activities *Fusion Eng. Des.* **89** 882–9
[4] Gibney E. 2019 UK hatches plan to build world's first fusion power plant *Nature*
[5] ITER Physics Expert Group on Divertor *et al* 1999 Power and particle control *Nucl. Fusion* **39** 2391–469
[6] Wenninger R. *et al* 2017 The DEMO wall load challenge *Nucl. Fusion* **57** 046002
[7] Ryutov D.D. 2007 Geometrical properties of a 'snowflake' divertor *Phys. Plasmas* **14** 064502
[8] Kotschenreuther M., Valanju P., Covele B. and Mahajan S. 2013 Magnetic geometry and physics of advanced divertors: the X-divertor and the snowflake *Phys. Plasmas* **20** 102507
[9] Valanju P.M., Kotschenreuther M., Mahajan S.M. and Canik J. 2009 Super-X divertors and high power density fusion devices *Phys. Plasmas* **16** 056110
[10] Stangeby P.C. *et al* 2000 *The Plasma Boundary of Magnetic Fusion Devices* vol 224 (Bristol: Institute of Physics Publishing)
[11] Lipschultz B., Goetz J.A., LaBombard B., McCracken G.M., Ohkawa H., Takase Y. and Terry J.L. 1997 Modification and control of divertor detachment in Alcator C-Mod *J. Nucl. Mater.* **241–243** 771–6
[12] Pitcher C.S., Carlson A.W., Fuchs C., Herrmann A., Suttrop W., Schweinzer J. and Weinlich M. (ASDEX Upgrade Team and Nbi Group) 1997 Routes to divertor detachment in ASDEX upgrade *J. Nucl. Mater.* **241–243** 696–700
[13] Havlíčková E., Harrison J., Lipschultz B., Fishpool G., Kirk A., Thornton A., Wischmeier M., Elmore S. and Allan S. 2015 SOLPS analysis of the MAST-U divertor with the effect of heating power and pumping on the access to detachment in the Super-x configuration *Plasma Phys. Control. Fusion* **57** 115001

[14] Reinke M.L. 2017 Heat flux mitigation by impurity seeding in high-field tokamaks *Nucl. Fusion* **57** 034004
[15] Hutchinson I.H. 1994 Thermal front analysis of detached divertors and MARFEs *Nucl. Fusion* **34** 1337
[16] Lengyel L. 1981 Analysis of radiating plasma boundary layers *Tech. Rep.* Max-Planck-Institut für Plasmaphysik
[17] Moulton D., Harrison J., Lipschultz B. and Coster D. 2017 Using SOLPS to confirm the importance of total flux expansion in Super-X divertors *Plasma Phys. Control. Fusion* **59** 065011
[18] Fishpool G. *et al* 2013 MAST-upgrade divertor facility and assessing performance of long-legged divertors *J. Nucl. Mater.* **438** S356–9
[19] Cowley C. 2022 *OptimisingDetachmentControl_Routines* (Online available: http://dx.doi.org/10.5281/zenodo.6577438)
[20] Harrison J.R. *et al* 2017 Detachment evolution on the TCV tokamak *Nucl. Mater. Energy* **12** 1071–6
[21] Theiler C. *et al* 2017 Results from recent detachment experiments in alternative divertor configurations on TCV *Nucl. Fusion* **57** 072008
[22] Moulton D., Stangeby P.C., Bonnin X. and Pitts R.A. 2021 Comparison between SOLPS-4.3 and the Lengyel model for ITER baseline neon-seeded plasmas *Nucl. Fusion* **61** 046029
[23] Rozhansky V., Molchanov P., Veselova I., Voskoboynikov S., Kirk A. and Coster D. 2012 Contribution of drifts and parallel currents to divertor asymmetries *Nucl. Fusion* **52** 103017
[24] Kallenbach A. *et al* 2013 Impurity seeding for tokamak power exhaust: from present devices via ITER to DEMO *Plasma Phys. Control. Fusion* **55** 124041